Dynamics in Secondary Metabolite Gene Clusters in Otherwise Highly Syntenic and Stable Genomes in the Fungal Genus *Botrytis*

Claudio A. Valero-Jiménez[1], Maikel B.F. Steentjes [1], Jason C. Slot [2], Xiaoqian Shi-Kunne[1], Olga E. Scholten[3], and Jan A.L. van Kan [1],*

[1]Laboratory of Phytopathology, Wageningen University, The Netherlands
[2]Department of Plant Pathology, The Ohio State University
[3]Plant Breeding, Wageningen University & Research, The Netherlands

*Corresponding author: E-mail: jan.vankan@wur.nl.

Abstract

Fungi of the genus *Botrytis* infect >1,400 plant species and cause losses in many crops. Besides the broad host range pathogen *Botrytis cinerea*, most other species are restricted to a single host. Long-read technology was used to sequence genomes of eight *Botrytis* species, mostly pathogenic on *Allium* species, and the related onion white rot fungus, *Sclerotium cepivorum*. Most assemblies contained <100 contigs, with the *Botrytis aclada* genome assembled in 16 gapless chromosomes. The core genome and pan-genome of 16 *Botrytis* species were defined and the secretome, effector, and secondary metabolite repertoires analyzed. Among those genes, none is shared among all *Allium* pathogens and absent from non-*Allium* pathogens. The genome of each of the *Allium* pathogens contains 8–39 predicted effector genes that are unique for that single species, none stood out as potential determinant for host specificity. Chromosome configurations of common ancestors of the genus *Botrytis* and family Sclerotiniaceae were reconstructed. The genomes of *B. cinerea* and *B. aclada* were highly syntenic with only 19 rearrangements between them. Genomes of *Allium* pathogens were compared with ten other *Botrytis* species (nonpathogenic on *Allium*) and with 25 Leotiomycetes for their repertoire of secondary metabolite gene clusters. The pattern was complex, with several clusters displaying patchy distribution. Two clusters involved in the synthesis of phytotoxic metabolites are at distinct genomic locations in different *Botrytis* species. We provide evidence that the clusters for botcinic acid production in *B. cinerea* and *Botrytis sinoallii* were acquired by horizontal transfer from taxa within the same genus.

Key words: ancestral genome, horizontal transfer, necrotroph, secondary metabolite.

Significance

We sequenced the genomes of nine plant pathogenic Sclerotiniaceae fungi, most of them infecting onion or related *Allium* species, to identify host range determinants by analyzing what these species share and what distinguishes them from their non-*Allium* sister species. Despite being unable to identify host range determining genes, several exciting observations were made. Sclerotiniaceae have stable genomes with similar chromosome architecture. We reconstructed an ancestral genome for all Sclerotiniaceae that contained 16 core chromosomes, as do all extant species for which chromosome numbers are known. Nevertheless, two gene clusters for secondary metabolite biosynthesis were located in entirely different genomic environments in these species. Evidence is presented that one of these gene clusters has undergone horizontal transfer within the genus *Botrytis*.

Introduction

Fungi have great societal impact because of their utility for nutritional, industrial, and medical purposes, as well as their pathogenic behavior on humans and plants. In recent years, the sequencing of fungal genomes has progressed at tremendous pace thanks to their small genome size and decreases in sequencing costs (Spatafora et al. 2017). Many species of industrial fungi from the genera *Aspergillus*, *Penicillium*, and *Trichoderma* have been sequenced (e.g., de Vries et al. 2017), whereas for human pathogens such as *Cryptococcus neoformans*, *Candida* spp., or *Aspergillus fumigatus*, numerous isolates were sequenced to obtain insight in population diversity (e.g., Lind et al. 2017; Ashton et al. 2019). Similarly, many dozens of plant pathogenic fungi species have been sequenced in order to gain insight into their evolution and the traits that enable the infection of plants (Möller and Stukenbrock 2017). Studies on plant pathogenic fungi have provided evidence for evolutionary adaptations that confer dynamics and plasticity on the genome, such as the presence of repeat-rich, gene-poor genomic regions or the possession of entire "dispensable" or "lineage-specific" chromosomes that contain effector genes which confer the capacity to specifically infect certain host plant species or plant genotypes (Dong et al. 2015; Lo Presti and Kahmann 2017; Sipos et al. 2017; Bertazzoni et al. 2018).

The fungal genus *Botrytis* comprises ~35 recognized species that all are pathogenic on plants (Hyde et al 2014; Garfinkel et al. 2017) with the exception of *Botrytis deweyae*, which colonizes *Hemerocallis* (daylily) as an endophyte (Grant-Downton et al. 2014). *Botrytis* spp. are notorious pathogens with a necrotrophic infection behavior, that is, they kill host cells and invade the dead cells to acquire nutrients. Two species that have been extensively studied are *Botrytis cinerea* and *Botrytis pseudocinerea*, morphologically indistinguishable taxa that cause gray mold on >1,400 host plant species (Elad et al. 2016). Other *Botrytis* species are considered to be restricted to a single host or a small number of taxonomically related hosts (Elad et al. 2016; Staats et al. 2005). In these cases, each host plant usually is infected by its own specialized *Botrytis* species. There are two exceptions in the pattern of specialized host–pathogen relationships within the genus: as many as eight *Botrytis* species can infect onion (*Allium cepa*) or other *Allium* species (Staats et al. 2005), and a recent study reported as many as 15 previously unknown, phylogenetically distinct *Botrytis* taxa sampled from peony in Alaska (Garfinkel et al. 2019). Phylogenetic analysis separated the genus *Botrytis* into two distinct clades, and *Botrytis* species that infect *Allium* are widely dispersed throughout the largest clade (Staats et al. 2005; Hyde et al. 2014; Garfinkel et al. 2019). Their closest relatives are often pathogenic on hosts that are phylogenetically distant from *Allium*. For example, the closest relatives of *Botrytis squamosa* (onion leaf blight) are the lily pathogen *Botrytis elliptica* and *Hemerocallis* endophyte B.

deweyae. Furthermore, the closest relative of *Botrytis aclada* (onion neck rot) is the peony pathogen *Botrytis paeoniae*. By contrast, *Botrytis globosa* and *Botrytis sphaerosperma* are sister taxa and both able to infect *Allium* hosts. The fact that *Allium* pathogens are dispersed over the phylogeny of the genus *Botrytis* suggests that the capacity to infect *Allium* has either been acquired multiple times or lost multiple times, independently, during evolution in the genus.

Pathogens with a necrotrophic lifestyle such as *Botrytis* spp. actively manipulate the cell death balance in their host plant, and in the necrotrophic phase exploit the host cell death machinery by secreting cell death-inducing metabolites and effector proteins (Veloso and van Kan 2018). In the necrotrophic wheat pathogen *Parastagonospora nodorum*, several cell death-inducing effector proteins were identified that contribute to pathogenicity only on wheat genotypes carrying a cognate receptor for these effectors, following an inverse gene-for-gene interaction (Liu et al. 2009, 2012; Faris et al., 2010; Shi et al. 2015, 2016). Each effector–receptor pair contributes in a quantitative manner to disease severity. At least one of the *Parastagonospora nodorum* effector genes has been horizontally transferred between distinct fungi pathogenic on wheat and barley (Friesen et al. 2006; McDonald et al. 2019).

The genome of the generalist *B. cinerea* has been extensively studied in the past decade. A gapless genome assembly was generated comprising 18 contigs, representing (near-)full-length chromosomes. Two contigs are minichromosomes (209 and 247 kb, respectively) with few genes and neither seems relevant for plant infection (van Kan et al. 2017), indicating that the core genome of *B. cinerea* consists of 16 chromosomes. Light microscopic studies by Shirane et al. (1989) showed that five *Botrytis* species (*B. aclada*, *B. byssoidea*, *B. cinerea*, *B. squamosa*, and *B. tulipae*) all contain 16 mitotic chromosomes. The *B. cinerea* reference assembly was supported by a genetic and optical map (van Kan et al. 2017) and a manually curated community annotation (Ensembl Fungi; Pedro et al. 2019). In a follow-up study, we analyzed the genomes of nine *Botrytis* species, mainly pathogens on flower bulb crops, using short-read sequence technology (Valero-Jiménez et al. 2019). In the present study, we sequenced the genomes of eight additional host-specific *Botrytis* species and one *Sclerotium* species, most of which are pathogenic on *Allium*, in order to compare their predicted proteome content and possibly identify host range determinants. The comparison focused on genes that are present in (and possibly shared among) *Allium* pathogens and absent from the non-*Allium* pathogens. The genome assemblies were of sufficiently high quality to analyze chromosome architecture and synteny and to infer the genome organization of ancestors of the genus *Botrytis* and the family Sclerotiniaceae. Furthermore, analysis of secondary metabolite (SM) biosynthetic gene clusters (BGCs) in Sclerotiniaceae and 25 other fungi within the Leotiomycetes showed a patchy

distribution of these clusters and provided evidence for two horizontal transfer events of an SM BGC within the genus *Botrytis*.

Materials and Methods

Strains and Culture Conditions

The fungal isolates that were sequenced are listed in supplementary table S1, Supplementary Material online. For long-term storage, all *Botrytis* species were kept as conidial suspensions in 15% glycerol at −80 °C, whereas *Sclerotium cepivorum* was stored as sclerotia at room temperature. The fungi were grown on malt extract plates at 20 °C before DNA extraction.

DNA and RNA Isolation

High molecular weight DNA was isolated from freeze-dried and grinded mycelium upon treatment with cell lysis solution (Qiagen), proteinase K, and protein precipitation solution (Qiagen). DNA was precipitated using isopropanol, redissolved in Tris–ethylenediaminetetraacetic acid buffer, and treated with RNase A. The obtained DNA was cleaned using a Salt: chloroform wash (Pacific Biosciences shared protocol).

RNAs used for producing RNA-Seq libraries were pools of RNA isolated from different sources: 1) 5-day old mycelia grown on malt extract plates supplemented with blended onion leaves, 2) conidia, 3) sclerotia, 4) infected onion bulbs, and 5) infected onion leaves. For isolation of RNA, freeze-dried, grinded samples were incubated in Trizol (Ambion, Life Technologies) and treated with chloroform. After adding ethanol to the aqueous phase, the mixture was used as input for an RNeasy Plant Mini Kit (Qiagen) to isolate RNA.

Sequencing and Assembly

All genomes were sequenced with one Pacbio SMRT cell using the Sequel instrument at Keygene N.V. (Wageningen, the Netherlands). De novo assembly was done with HGAP (Chin et al. 2013) and CANU (Koren et al. 2017) using default settings. The resulting assemblies were combined with quick-merge (Chakraborty et al. 2016), then two steps of corrections were done with Arrow, and erroneously merged contigs (based on inspection of mapped reads coverage) were manually corrected. Completeness of the genome assembly was assessed by the Benchmarking Universal Single-Copy Orthologs (BUSCO) (Simão et al. 2015). The transcriptome of each genome was sequenced using strand-specific paired-end libraries with a read length of 2× 150 bp using an Illumina HiSeq-X sequencer at the Beijing Genome Institute (BGI, Hongkong, China).

Genome Annotation

Genome annotation was performed using the FUNGAP pipeline (Min et al. 2017), which included the annotation by MAKER (Cantarel et al. 2008), AUGUSTUS (Stanke et al. 2006), and BRAKER (Hoff et al. 2016). The gene prediction tools were supported with RNA-Seq libraries. Gene models of the manually curated genome of *B. cinerea* (van Kan et al. 2017), and all the fungal proteins available in the Swissprot database were provided as evidence for gene prediction. Furthermore, the predicted proteins were manually inspected and curated. The genome curation was done in Webapollo (Dunn et al. 2019), and each gene was inspected to confirm that prediction was supported by the evidence tracks (RNA-Seq, *B. cinerea* as reference and the Swissprot proteins); for instance, some gene models were deleted if they were overlapping a repetitive region, whereas other gene models were changed to have a correct Methionine start, or correct splice junctions. The manual curation was done to all the predicted proteins of *B. aclada*, *B. squamosa*, and *S. cepivorum*, and to the secretome of all other genomes. The predicted proteins were functionally annotated using the funannotate pipeline (Love et al. 2019).

Phylogenetic and Phylogenomic Analysis

The phylogenetic relationships of the *Botrytis* genus and other related species of Sclerotiniaceae were determined between all species sequenced in this study and including the previously sequenced species *B. cinerea* B05.10 (van Kan et al. 2017), and other *Botrytis* species (Valero-Jiménez et al. 2019). The other species that were included were *Sclerotinia sclerotiorum* and *Sclerotinia borealis*, and *Marssonina brunnea* as the outgroup of the tree. The tree was constructed using 4,746 single-copy ortholog genes, identified with Orthofinder (Emms and Kelly 2015). The protein sequence for each gene was aligned and concatenated into a single matrix using MAFFT (Katoh and Standley 2013), and a maximum-likelihood phylogenetic tree was inferred with RAxML v.8.2.10 (Stamatakis 2014) using a generalized time reversible plus GAMMA amino acid substitution model with 100 rapid bootstraps. A pan-genome analysis was done to calculate the number of core genes and was estimated using OrthoMCL (Li 2003) implemented in GET_HOMOLOGUES-EST (Contreras-Moreira and Vinuesa 2013) with e-value $1e^{-5}$ and 75% coverage. For the pan-genome analysis, only the orthogroups present in at least two species were included.

Secretome and Effector Prediction

Genes encoding putatively secreted proteins were identified for each genome using several prediction tools. Signal-P v4.1 (Petersen et al. 2011) was initially used to screen for a signal peptide, followed by TMHMM v.2.0 (Krogh et al. 2001) to identify putative transmembrane domains. Proteins that did

not have a signal peptide or that had a transmembrane domain (a single transmembrane domain in the first 60 amino acids was allowed) were discarded. TargetP was used to predict protein localization (Emanuelsson et al. 2007). Effectors were predicted using the EffectorP tool v1.0 and v2.0 (Sperschneider et al. 2016).

Ancestral Genome Reconstruction

The ancestral genome of *Botrytis* was constructed using the CHROnicle package that comprises SynChro, ReChro, and Anchro (Vakirlis et al. 2016). In order to identify conserved synteny blocks, pairwise comparisons between the genomes were done with SynChro. Subsequently, reconstruction of the ancestral chromosome gene order was done with Anchro.

SM Gene Cluster Analysis

Putative gene clusters that are predicted to be involved in biosynthesis of SMs were identified using antiSMASH using default settings (antibiotics and Secondary Metabolite Analysis SHell) version 4.0.1 (Weber et al. 2015). The data set used for this analysis included 45 genomes from the order Leotiomycetes that were publicly available and published (supplementary table S3, Supplementary Material online). BiG-SCAPE version 20181005 (Navarro-Muñoz et al. 2020) was used to analyze all the SMs clusters predicted by antiSMASH. In the BiG-SCAPE analysis, a cutoff of 0.65 as well as the MIBiG parameter that included the MIBiG repository version 1.4 of annotated SMC was used (Medema et al. 2015). The output of BiG-SCAPE was visualized using Cytoscape version 3.7.1 (Shannon et al. 2003).

Reconstruction of BGC Evolution

Presence/absence and additional fragmented homologs of BOT and BOA genes for each species was confirmed by TBlastN against the genome assemblies (supplementary data S5 and S6, Supplementary Material online). Pseudogenes were manually identified by inspection of TBlastN reports for in-frame stop codons, and interrupted reading frames and truncations that could not be explained by novel intron sites (supplementary data S5 and S6, Supplementary Material online).

Phylogenetic analyses were performed on all BGC genes, both with and without pseudogenes and outgroup taxa (supplementary data S7 and S8, Supplementary Material online). Outgroup taxa were obtained by searching a database of 529 genome annotations (Gluck-Thaler and Slot 2018) using BlastP. Protein sequence data sets for each gene were aligned using mafft v. 7.221 (Katoh and Standley 2013), and ambiguously aligned characters were removed using TrimAl v. 1.4 (Capella-Gutiérrez et al. 2009). Maximum-likelihood analysis was performed in RAxML v. 8.2.9 (Stamatakis 2014) with automated model selection and topological robustness was

assessed by 100 bootstrap replicates. In order to evaluate alternative hypotheses versus inferred horizontal gene transfer (HGT) events, we applied minimal topological constraints to exclude putative transferred genes from the donor clade. Constrained trees (supplementary data S9, Supplementary Material online) were built with automated model selection and their likelihoods were compared using the Approximately Unbiased test with 10,000 multiscale bootstrap replicates (Shimodaira 2002) as implemented in IQ-TREE v. 1.6.12 (Nguyen et al. 2015).

In order to determine synteny in the BOT and BOA loci (supplementary data S10, Supplementary Material online), each locus including up to ten genes on either side of the BOA/BOT genes of interest (if present) was combined and assigned to a homology group using usearch cluster_agg method with a minimum linkage identity of 0.6 in usearch v. 8.0.1517 (Edgar 2010). The loci were then manually aligned according to their homology group and manual blasts were performed to confirm true orthology where ambiguous.

Ancestral state reconstructions (supplementary data S11, Supplementary Material online) were performed using a substitution matrix weighted against gain of functional genes and pseudogenes, except where HGT was already determined by gene trees and synteny analysis for BOA clusters in Mesquite v 3.6 (Maddison WP and Maddison DR 2019).

Results

Sequencing and Assembly

Eight *Botrytis* species and *S. cepivorum* (supplementary table S1, Supplementary Material online) were sequenced using long-read single-molecule technology at 34–120× coverage. The genome assembly sizes ranged from 42.98 to 61.28 Mb (table 1). The genomes of six species are similar in size to the previously described genome of *B. cinerea* (43.5 Mb; van Kan et al. 2017), whereas genomes of *B. squamosa*, *B. sinoallii*, and *S. cepivorum* exceed a size of 54 Mb. The *B. aclada* genome could be assembled into 16 distinct chromosomes, with eight chromosomes containing telomeric repeats at both ends, and six containing a telomeric repeat on one end.

The most fragmented assembly of the nine species is that of *B. elliptica*, despite its genome size of <48 Mb, with 137 contigs and a contig N50 of 652 kb. BUSCO analysis indicated that all genomes had a high level of completeness (98.0–99.2%). Prediction of gene models was performed using the FunGAP pipeline and supported by RNA-Seq data (from in vitro samples and infected plant material) and by alignment to the manually curated genome of *B. cinerea* B05.10 (van Kan et al. 2017). After prediction by this pipeline, proteomes of *B. aclada*, *B. squamosa*, and *S. cepivorum* were entirely manually curated, whereas for the other six species, only the (predicted) secreted proteins were manually curated.

Table 1

Assembly and Gene Prediction Information of *Botrytis* spp. Genomes from This Study

| Species	Contigs	Assembly Size (Mb)	Largest Contig (kb)	N50 (kb)	BUSCO Complete/ Partial	Predicted Genes	Secretome Size	% of Secreted Proteins
Botrytis byssoidea[a]	59	42.98	2,599	1,263	98.0 (99.3)	12,212	898	7.35
Botrytis globosa[a]	27	45.68	4,093	2,511	98.0 (99.0)	12,073	864	7.16
Botrytis elliptica[a]	137	47.66	2,119	652	99.2 (99.9)	12,442	932	7.49
Botrytis squamosa[a]	29	54.60	4,659	2,938	98.7 (99.1)	11,963	897	7.5
Botrytis deweyae[a]	76	44.36	2,431	1,076	98.0 (99.0)	12,480	942	7.55
Botrytis sinoallii[a]	47	61.28	6,466	2,252	98.3 (99.5)	12,281	885	7.21
Botrytis porri[a]	31	46.78	4,253	2,706	98.2 (98.9)	12,088	888	7.35
Botrytis aclada[a]	16	48.31	4,155	3,028	99.1 (99.3)	11,870	867	7.30
Sclerotium cepivorum[a]	48	55.66	4,533	1,651	98.2 (99.5)	11,107	790	7.11

[a]Taxa in the table are ordered as they appear in the phylogenetic tree in figure 1.
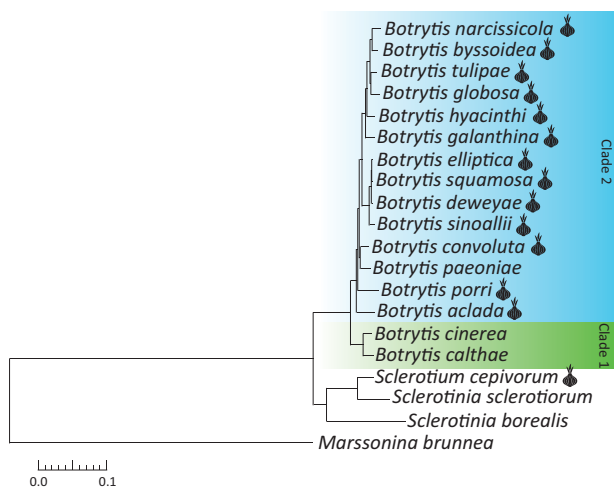
Fig. 1.—Phylogenetic tree based on single-copy orthologous genes of different *Botrytis* species and three Sclerotiniaceae, with *Marssonina brunnea* as the outgroup to root the tree. All branches have a high bootstrap support (ML > 90). Two clades previously reported in the genus *Botrytis* are highlighted. The bulb symbols next to the species names indicate species that infect monocotyledonous bulbous plants, species without symbol infect dicot hosts.

The curated proteomes of the nine species contain between 11,107 and 12,480 genes (table 1).

Phylogenetics and Phylogenomics

A phylogenetic tree was constructed based on a concatenated amino acid alignment of 4,746 conserved core genes totaling 409,576 positions, using *Marssonina brunnea* (order Helotiales, family Dermataceae) as the outgroup (fig. 1). The relationship among the *Botrytis* species is fully concordant with previous studies (Staats et al. 2005; Hyde et al. 2014), which divided the genus in two clades based on three protein-coding genes (G3PDH, HSP60, and RPB2). All *Botrytis* species newly sequenced in this study group in Clade 2, which contains taxa that mostly infect monocot

host plants (only *B. paeoniae* infects dicots). A pan-genome analysis for 16 *Botrytis* species (eight species sequenced in this study, seven species previously sequenced with short-read technology [Valero-Jiménez et al. 2019], and the previously sequenced *B. cinerea* B05.10 [van Kan et al. 2017]) indicated that the core genome of *Botrytis* spp. consists of 7,524 orthogroups (>60% of genes within any individual species; supplementary fig. S1a, Supplementary Material online), whereas the pan-genome consists of 13,856 orthogroups (supplementary fig. S1b, Supplementary Material online).

Analysis of Secreted Proteins

Secreted proteins are important tools of plant pathogenic fungi to either manipulate the physiology and immune responses of their host plants (effector proteins) or decompose the plant tissue that they colonize in order to acquire carbohydrate nutrients (plant cell wall degrading enzymes, PCWDEs). Orthologous groups of all secreted proteins from 16 *Botrytis* species sequenced in this work, as well as previously published (van Kan et al. 2017; Valero-Jiménez et al. 2019) and *S. cepivorum* were determined using Orthofinder. From a total of 14,838 proteins, 14,326 were assigned to 1,116 orthologous groups (supplementary data S1, Supplementary Material online). From these, 376 orthologous groups are shared among all 17 species (supplementary fig. S2, Supplementary Material online). Besides orthologous groups shared by all species, 171 groups (columns 2–18 in supplementary fig. S2, Supplementary Material online) are common to all species but one, whereas 454 orthologous groups are unique to a single species (columns 19–37 in supplementary fig. S2, Supplementary Material online). The secretome of *S. cepivorum* lacks 55 secreted proteins that are present in all *Botrytis* species and contains 83 singletons that are unique to *S. cepivorum*, as to be expected for a species from a distinct genus in the same family.

In view of the relevance of secreted effector proteins in fungus–plant interactions, an effector prediction was performed on the set of secreted proteins discussed above. For

each of the 16 *Botrytis* species and *S. cepivorum*, a total of 121–152 candidate effector genes was identified which were assigned to 244 orthologous groups (supplementary data S2, Supplementary Material online). Among these groups, 25 are represented in all 17 species and another 25 are shared among all but one species. On the other hand, each of the 17 species contains between 8 and 39 predicted effector genes that remained unassigned to orthologous groups, because they are unique for that single species. There were no predicted effectors which are shared among *Allium* pathogens but absent from non-*Allium* pathogens. Furthermore, pairwise comparisons between related *Botrytis* species with distinct hosts did not identify any effector genes that stood out as potential determinants for host specificity.

We also analyzed the secreted proteins that are related to the degradation of plant cell wall carbohydrates (supplementary table S2, Supplementary Material online). The genomes of 16 *Botrytis* spp. and *S. cepivorum* contain between 109 and 132 PCWDEs. *Sclerotium cepivorum* has fewer PCWDE-encoding genes than the *Botrytis* species. The PCWDEs were further subdivided depending on their substrate: cellulose, hemicellulose, or pectin. The numbers of secreted enzymes capable of degrading cellulose, hemicellulose, and pectin were mostly similar among *Botrytis* spp., with some deviations: *B. sinoallii* has notably fewer genes encoding pectinases (22 vs. 27–38 for other species; supplementary table S2, Supplementary Material online).

SM Gene Clusters

Fungi produce a wide array of SMs, usually synthesized by proteins encoded by genes that are physically clustered in the genome, referred to as SM BGCs (Keller et al. 2005). SMs contribute to the adaptation and survival in different environments and in the competition with other (micro)organisms (e.g., Chatterjee et al. 2016). In a previous study on nine *Botrytis* genomes assembled from short sequence reads, a patchy absence/presence pattern was observed for orthologs to BGCs that were functionally annotated in *B. cinerea* (Valero-Jiménez et al. 2019). Because of the fragmented assemblies resulting from short-read sequencing technology, the latter analysis only considered SM key biosynthetic enzymes, but not the entire gene cluster. In the present study, the analysis of SM gene clusters was extended to all 16 *Botrytis* species (short- and long-read technology based), four related taxa from the family Sclerotiniaceae, and 25 other taxa from the class Leotiomycetes, for which an annotated genome was publicly available (supplementary table S3, Supplementary Material online). The analysis was conducted by predicting BGCs in all 45 genomes using AntiSMASH, and grouping them by families using BiG-SCAPE. The 45 Leotiomycete genomes each contained between 3 and 67 BGCs (supplementary data S3, Supplementary Material online). The 1,571 BGCs were grouped over 438 BGC families

(supplementary data S4, Supplementary Material online), which were further categorized based on their phylogenetic distribution. Category 1 contains 342 families of SM BGCs that are distributed among taxa across Leotiomycetes. This category includes a few BGCs that encode enzymes involved in biosynthesis of common metabolites such as melanin and siderophores, however, the exact chemical structures of compounds produced by the vast majority of BGCs in this category remain unknown. Category 2 contains 36 families of BGCs that are present in Sclerotiniaceae (including the genus *Botrytis*) but not represented in the other 25 Leotiomycete taxa. This category includes the BGCs encoding enzymes involved in production of botcinic acid, and other yet unknown compounds. Category 3 contains 60 families of BGCs that are unique to the genus *Botrytis*, such as the cluster involved in production of botrydial, however, all other SMs produced by the other 59 BGCs in this category are unknown.

BGCs are commonly annotated on the basis of the type of compound that is produced, often a polyketide (PKS), non-ribosomal peptide (NRPS), or terpene (TS). The evolutionary trajectory of BGCs can be complex, and the distribution of specific BGCs can be scattered throughout the fungal kingdom (Slot and Gluck-Thaler 2019). Several cases of HGT of BGCs have been documented in fungi (Campbell et al. 2012; Ropars et al. 2015; Reynolds et al. 2018; Navarro-Munoz and Collemare 2020). We examined the distribution of the predominant classes of BGCs (PKS, NRPS, and TS) over the 45 Leotiomycete species analyzed (fig. 2 for PKS; supplementary fig. S3, Supplementary Material online, for NRPS; supplementary fig. S4, Supplementary Material online, for TS).

The distribution of BGCs is largely consistent with phylogenetic patterns, with related fungal taxa containing a similar distribution. A set of 20 PKS families (as identified by BiG-SCAPE) are most abundant in *Botrytis* species. Six families from this set are exclusive to *Botrytis* (highlighted red in fig. 2), whereas 14 families are also present in other Sclerotiniaceae or in more distantly related Leotiomycete taxa (highlighted in ocher). Conversely, a set of nine PKS clusters that are most abundant in Leotiomycetes outside the family Sclerotiniaceae have sparse and patchy distributions within the genus *Botrytis* (highlighted in blue).

Botrytis species possess at least five (*Botrytis convoluta*) and at most 11 (*B. cinerea*) NRPS clusters (supplementary fig. S3, Supplementary Material online). Five families of NRPS clusters are unique to the genus *Botrytis* (supplementary fig. S3, Supplementary Material online, highlighted in red), whereas eight other families are largely confined to the family Sclerotiniaceae, although two of them (FAM_02547 and FAM_02047) are also shared with the distant taxa *Phialophora hyalina* or *Phialocephala scopiformis* (supplementary fig. S3, Supplementary Material online, highlighted in ocher). Notably, *B. cinerea* contains two NRPS clusters that are not shared with any other *Botrytis* species but have orthologs in several distant Leotiomycetes (supplementary fig. S3,
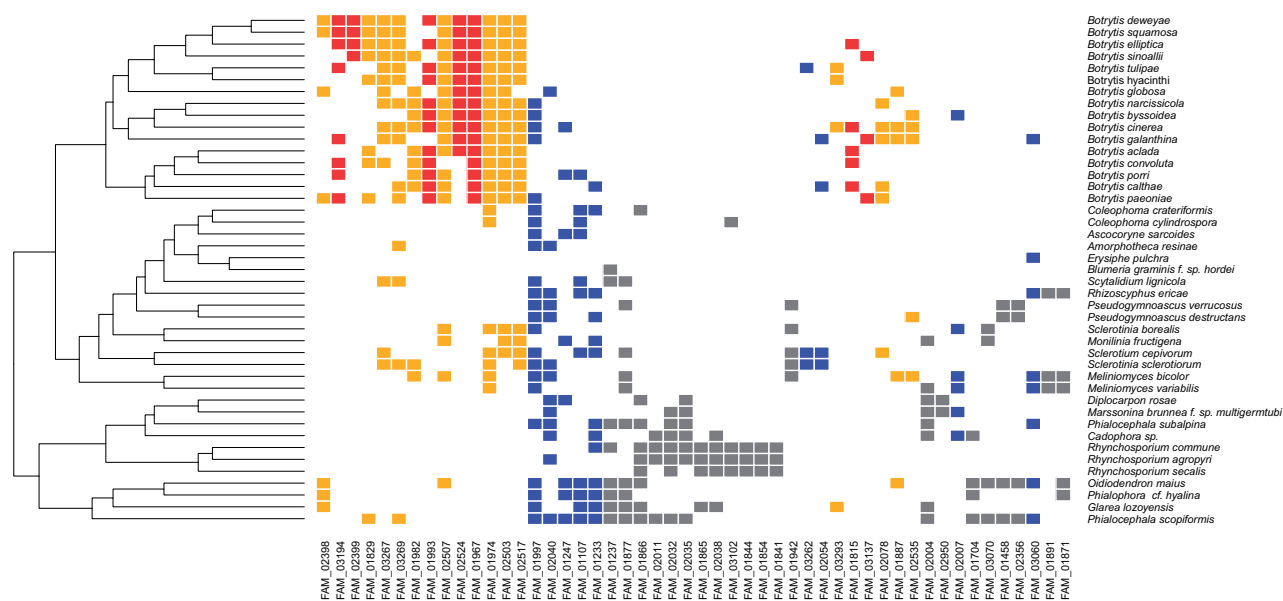
Fig. 2.—Distribution of polyketide synthase clusters in 45 Leotiomycetes. The 50 clusters that are most abundant among the 45 Leotiomycetes taxa are displayed. Clusters that are exclusively represented in *Botrytis* are marked red; clusters predominantly in *Botrytis* but also in some other taxa are marked ocher; clusters predominantly in other taxa but also in some *Botrytis* species are marked blue; clusters lacking in all *Botrytis* spp. are marked gray.

Supplementary Material online, highlighted in blue). The families of terpene cyclase (TS) clusters are relatively simple in pattern, with each *Botrytis* species containing 3–6 TS cluster families (supplementary fig. S4, Supplementary Material online). Eight of the families are exclusively detected in *Botrytis* species (supplementary fig. S4, Supplementary Material online, highlighted in red), whereas four are also present in other Sclerotiniaceae, and two of the TS cluster families are even detected in distant Leotiomycetes (supplementary fig. S4, Supplementary Material online, highlighted in ocher). The family FAM_03197 is conserved in all Sclerotiniaceae, as well as in six other Leotiomycetes, whereas FAM_02531 is present in nine Sclerotiniaceae and six distant Leotiomycetes. Except for the family FAM_02168, involved in the synthesis of the phytoxic metabolite botrydial, the chemical nature of the products of these clusters is unknown.

Ancestral Genome Reconstruction of the Genus *Botrytis* and the Family Sclerotinaceae

The high quality of the long-read assemblies and the previously published *B. cinerea* genome, as well as the extensive manual curation effort of gene models, enabled us to perform a synteny analysis and a reconstruction of the ancestral chromosome configuration of the genus *Botrytis*, in order to understand the extent and nature of chromosomal rearrangements over the course of evolution of the extant species. *Botrytis elliptica* was excluded from the ancestor reconstruction for two reasons: first, the assembly was the most fragmented of all (137 contigs) and second, the phylogenetic relation of *B. elliptica* to its sister taxa *B. squamosa* and

B. deweyae could not be resolved (fig. 1), which hampered the analysis. The inferred ancestral genome of the entire genus *Botrytis* (AB0) consists of 17 syntenic blocks (fig. 3). Thirteen of the 16 *B. cinerea* core chromosomes are entirely syntenic to the AB0 ancestor, and 17 balanced rearrangements (mostly inversions) are inferred between the ancestor AB0 and the extant *B. cinerea* (table 2 and supplementary table S4, Supplementary Material online).

The A1 genome is the inferred ancestor of members of clade 2 in the genus *Botrytis*, whereas *B. cinerea* is the single representative of clade 1 in the analysis (fig. 1). The inferred A1 genome is identical to AB0 (fig. 3). The extant *B. aclada* genome contains ten rearrangements as compared with A1. The A2 intermediate ancestor was inferred to be derived from A1 upon fusion of A1 contigs 13 and 17, and fission of A1 contig 3 (resulting in A2 contigs 5 and 17). Downstream of the A3 intermediate ancestor, the interpretation becomes complex as numbers of contigs increase due to the more fragmented assemblies of some species, for example, *B. deweyae*, *B. byssoidea*, and *B. sinoallii*. Nonetheless, the number of contigs of intermediate ancestors remains 25 or lower and the number of rearrangements between nodes in the tree ranges from 3 to 43 (table 2).

Reconstruction of ancestral genomes was extended to the family Sclerotiniaceae using the genomes of *S. cepivorum* (this study) and *Sclerotinia sclerotiorum* (Derbyshire et al. 2017) (supplementary fig. S5, Supplementary Material online). Due to the more fragmented assembly of the *S. cepivorum* genome, the inferred common ancestor AS1 comprised 21 syntenic blocks, five of which were quite small and probably
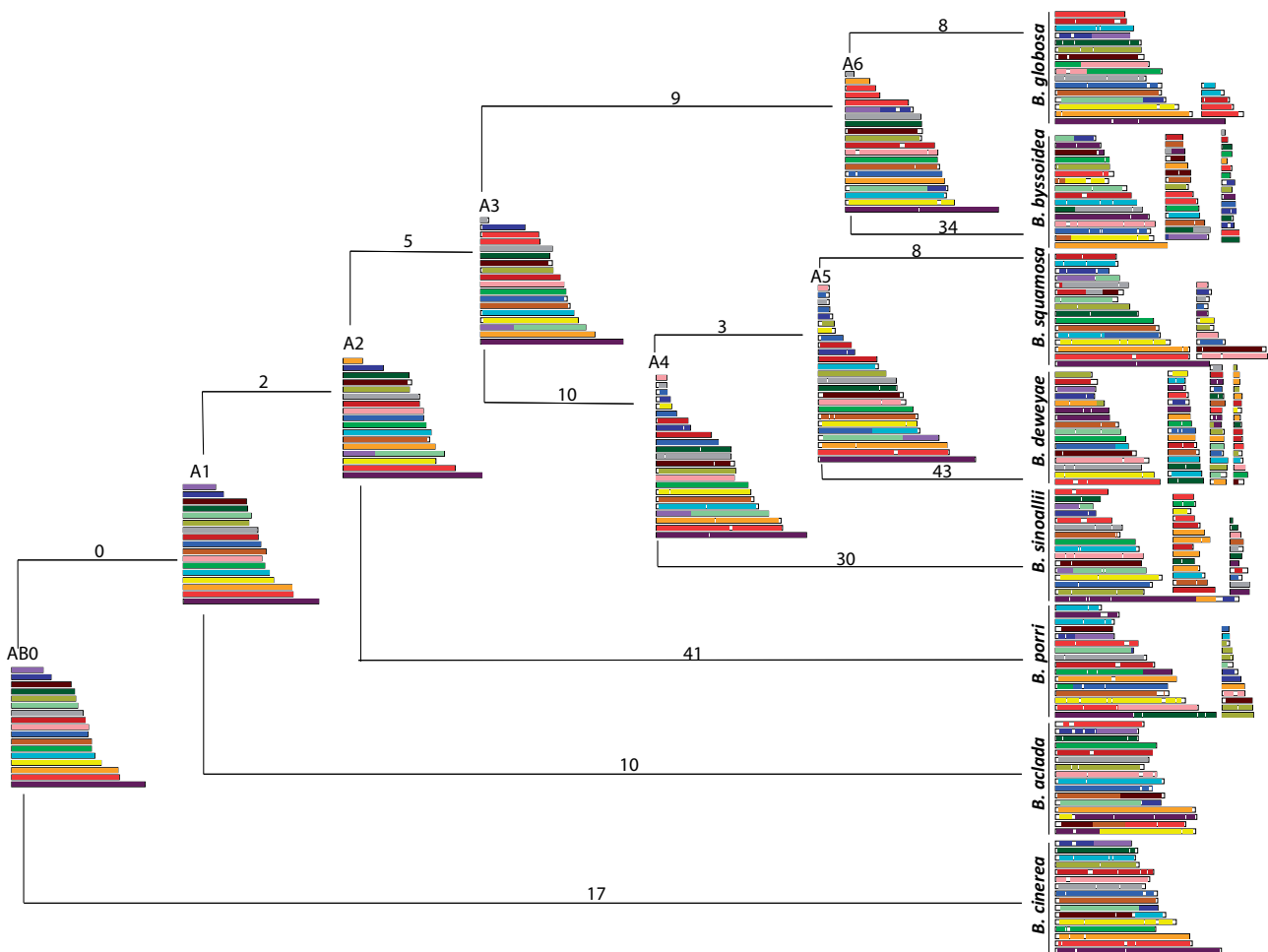
Fig. 3.—The most parsimonious evolutionary trajectory from the ancestral (A0) configuration toward extant *Botrytis* species. Colored boxes represent syntenic blocks. A1–A6 represent intermediate ancestors. Numbers above the branches represent the total number of balanced rearrangements (interchromosomal translocations and fusions/fissions; intrachromosomal inversions) accumulated between two genomes.

Table 2

Numbers of Balanced Genomic Rearrangements between Inferred Ancestral Genomes (AB0-A6) and Extant *Botrytis* Species, as Shown in Figure 3

	AB0-BCIN	AB0-A1	A1-BACL	A1–A2	A2–A3	A3–A4	A3–A6	A4–A5	A4-BSIN	A5-BSQU	A5-BDEW	A6-BBYS
Inversions	15	0	3	0	2	3	6	1	6	2	1	3
Translocations	1	0	1	0	0	0	1	0	2	2	0	4
Transpositions	1	0	1	0	0	0	0	0	1	0	0	0
Fusions	0	0	0	1	2	1	0	1	2	1	2	0
Fissions	0	0	5	1	1	6	2	1	19	3	40	27
Sum	17	0	10	2	5	10	9	3	30	8	43	34

Note.—Further details of the types of rearrangements are provided in supplementary table S4, Supplementary Material online. BCIN, *B. cinerea*; BACL, *B. aclada*; BSIN, *B. sinoallii*; BSQU, *B. squamosa*; BDEW, *B. deweyae*; BBYS, *B. byssoidea*.

represent only parts of chromosomes. However, the common ancestor ABS0 of the family Sclerotiniaceae contains 16 syntenic blocks, and the configuration of ABS0 differs from the ancestral *Botrytis* genome AB0 by just a single rearrangement (supplementary fig. S5, Supplementary Material online).

Synteny between *B. aclada* and *B. cinerea*

In order to explore genome rearrangements between individual species in more detail, we further examined the synteny between the genomes of *B. aclada* and *B. cinerea* (the most complete and best annotated) by pairwise alignments.
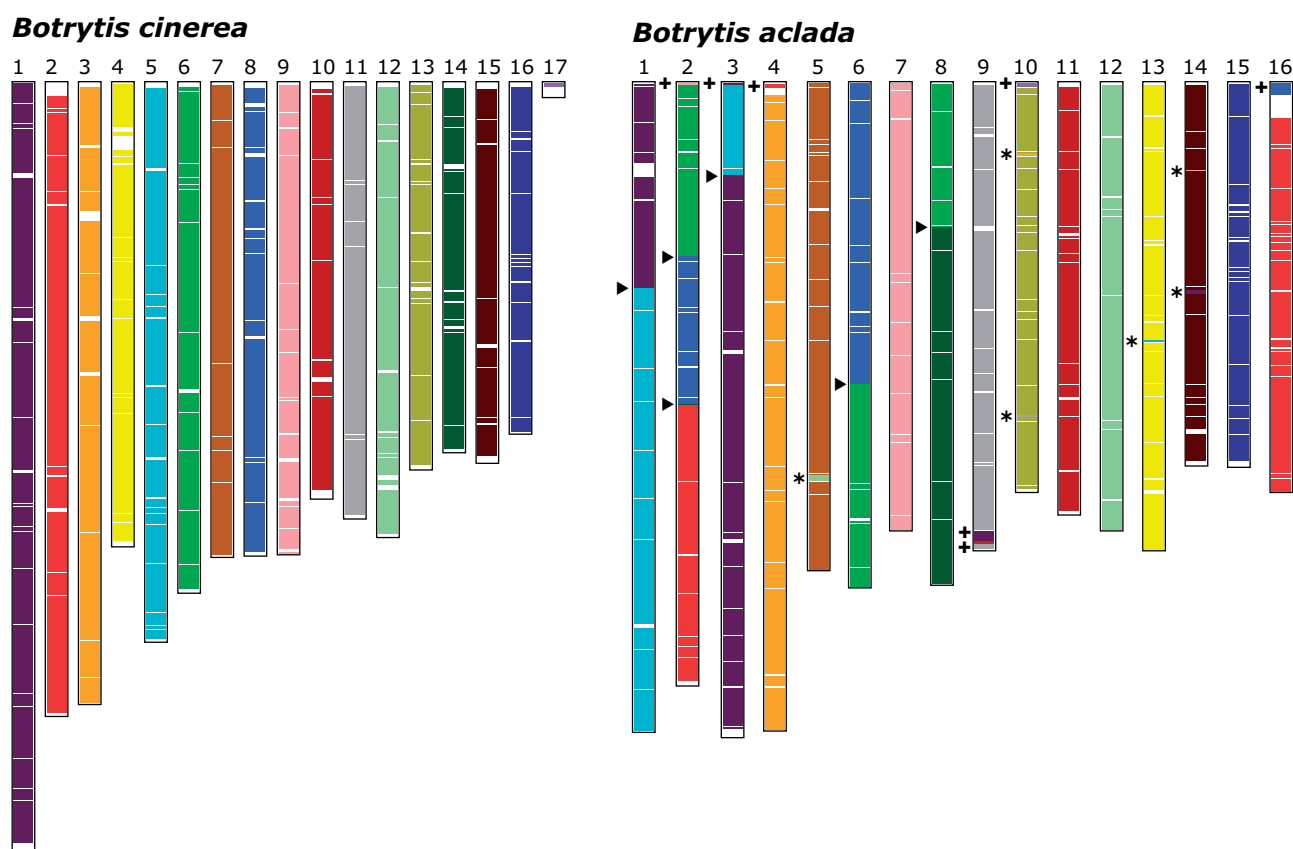
Fig. 4.—Synteny analysis between *Botrytis aclada* and *Botrytis cinerea*. The 17 chromosomes of *B. cinerea* are color-coded uniformly, the corresponding syntenic regions in *B. aclada* have identical colors. White regions reflect repetitive regions or lack of homology. Arrowheads indicate large reciprocal interchromosomal rearrangements. Asterisks indicate small interchromosomal transpositions. Plus symbols indicate interchromosomal telomeric translocations. Intrachromosomal inversions are not indicated.

Botrytis cinerea minichromosome 18 (BCIN18) was excluded from this analysis because it contains only 13 genes, none of which is orthologous to genes in *B. aclada.* The second minichromosome of *B. cinerea*, BCIN17, did show some homology to the tip of BACL10 and was therefore included in the analysis. Graphical representation of the alignment (fig. 4) reveals that four chromosomes represent fully syntenic blocks, though some of these blocks contain segmental inversions of ancestral regions on the same chromosome (not visible in the color display). In the remaining 12 chromosomes, the alternation of colored boxes reflects the occurrence of six interchromosomal rearrangements, as well as 13 small translocations or transpositions, of which seven occurred at or close to the telomeres (fig. 4).

Strikingly, we noted that SM BGCs were present in some of these translocated segments. Specifically, BACL05 is almost perfectly syntenic to BCIN07, with the exception of an insertion of a cluster of seven genes (fig. 4, green box marked by an asterisk) representing the BGC for the sesquiterpene metabolite botrydial (Siewers et al. 2005; Pinedo et al. 2008; Porquier et al. 2016), which in *B. cinerea* is located in

BCIN12. Conversely, the only difference between BACL12 and BCIN12 is the insertion (in BCIN12) of a segment that exactly contains the BGC for botrydial. Furthermore, BACL9 is entirely syntenic to BCIN11, however, it contains an insertion of the BGC for the phytotoxic metabolite botcinic acid (Dalmais et al. 2011; Porquier et al. 2019) close to the 3'-telomeric region, which in *B. cinerea* is located at the start of BCIN01 (van Kan et al. 2017).

Genomic Locations of Botrydial and Botcinic Acid BGCs

The synteny analyses described above provided indications that SM BGCs occur in regions that possibly underwent translocation at some moment in the evolution of *Botrytis* species. The distribution of botrydial (BOT) and botcinic acid (BOA) BGCs over the Sclerotiniaceae and the genus *Botrytis* appeared to be patchy. Specifically, the BOT cluster is present in eight *Botrytis* species and absent in other Sclerotiniaceae. We compared the BOT clusters and their flanking sequences in seven species: *B. aclada, B. cinerea, B. elliptica, B. deweyae, B. porri, B. sinoallii,* and *B. squamosa.* The *B. peaoniae*
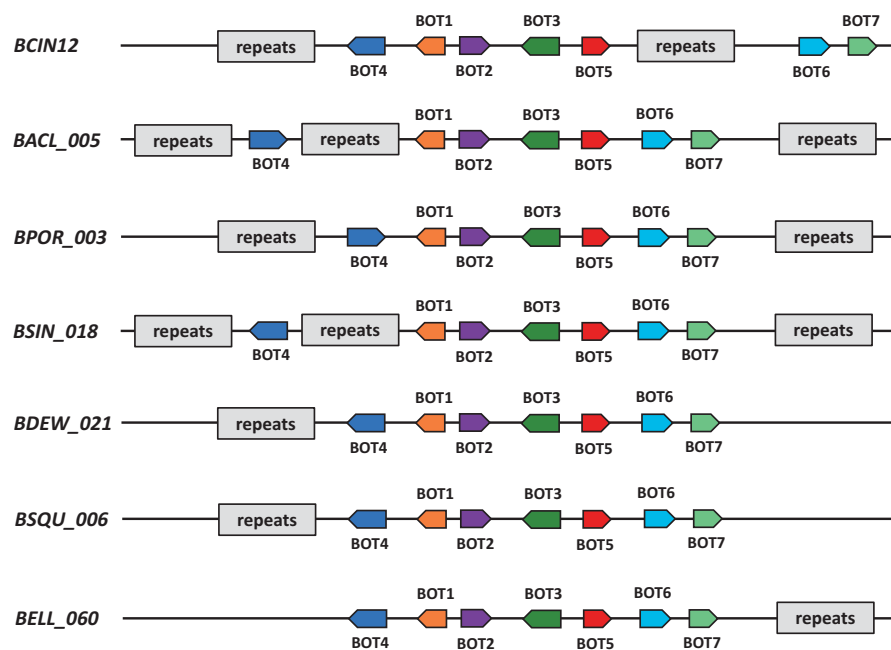
Fig. 5.—Organization of BOT clusters in seven *Botrytis* species. BCIN, *B. cinerea*; BACL, *B. aclada*; BPOR, *B. porri*; BSIN, *B. sinoallii*; BSQU, *B. squamosa*; BDEW, *B. deweyae*; BELL, *B. elliptica*. The number of the contig is given behind the species name tag. The seven BOT gene orthologs (not drawn to scale) are color-coded uniformly; the arrow indicates direction of transcription. Repeats are indicated with a gray box. Repeats are not drawn to scale and range in length from 1 to 160 kb.

genome, though containing a BOT cluster, was sequenced by Illumina technology (Valero-Jiménez et al. 2019) and its assembly was too fragmented for synteny analysis. The order of the genes BcBOT1–7 within the cluster was identical in all species, however, the most upstream gene (BcBOT4), was in inverted orientation in *B. aclada* and *B. porri* as compared with the other five species (fig. 5). The BOT clusters were in all cases flanked by gypsy/copia repeats, with lengths up to 160 kb, either on one side (*B. cinerea*, *B. deweyae*, *B. elliptica*, and *B. squamosa*), or on both sides (*B. porri*, *B. aclada*, and *B. sinoallii*) and some species even contained internal transposon repeats within the BOT cluster (*B. aclada*, *B. cinerea*, and *B. sinoallii*; fig. 5). Based on the RNA-Seq reads used for structural annotation, it was observed that all species that do contain intact BOT clusters express all of the seven genes. As these expression data were based on pooled RNAs, representing multiple fungal tissue types and infection stages, it was not possible to compare the expression levels between species or to determine under which conditions the genes were expressed.

The BOA cluster was detected, in whole or in part, in all but one *Botrytis* species (*B. paeoniae*), and in *Sclerotinia sclerotiorum* as well as *S. cepivorum*. In many cases, the BOA cluster in *Botrytis* species is located close to the end of a contig. It was previously reported that in *B. cinerea*, the BOA cluster is at the very start of BCIN01, only 5 kb away from the telomere (van Kan et al. 2017). Alike for the BOT clusters mentioned above, all species that contain intact BOA clusters express all of the 13 genes, however, the use of pooled RNAs prevented us from

comparing expression levels between species or determine under which conditions the genes were expressed.

In view of the high synteny between *Botrytis* species, we examined whether the BOT and BOA clusters in the different species are in syntenic locations as compared with *B. cinerea*. Surprisingly, analysis of flanking genes revealed that BOT clusters are in four distinct genomic regions in the seven *Botrytis* species analyzed. None of the species other than *B. cinerea* contained the BOT cluster in a region syntenic to BCIN12 (fig. 6). The genes directly flanking the BOT cluster in *B. cinerea* (Bcin12g06360 and Bcin12g06440) in all but one of the six species have orthologs that are directly adjacent to one another in these genomes, with intergenic regions ranging from 2 to 5 kb.

No indication was found for the occurrence of truncated remnants of BOT genes at this position in the six genomes. Also in all but one of the other species lacking a BOT cluster, orthologs to Bcin12g06360 and Bcin12g06440 are directly adjacent to one another in these genomes. Through similar analyses and reasoning, the BOT cluster in *B. aclada* is present in a unique position that is syntenic to BCIN07, whereas the BOT cluster in *B. porri* is present in a unique position that is syntenic to positions in five other species (all except in *B. cinerea*, where a synteny break has occurred); lastly, the BOT clusters in *B. squamosa*, *B. deweyae*, *B. elliptica*, and *B. sinoallii* are all located in a syntenic genomic region, which is equivalent to a location between Bcin08g05830 and Bcin08g05810 (fig. 6).
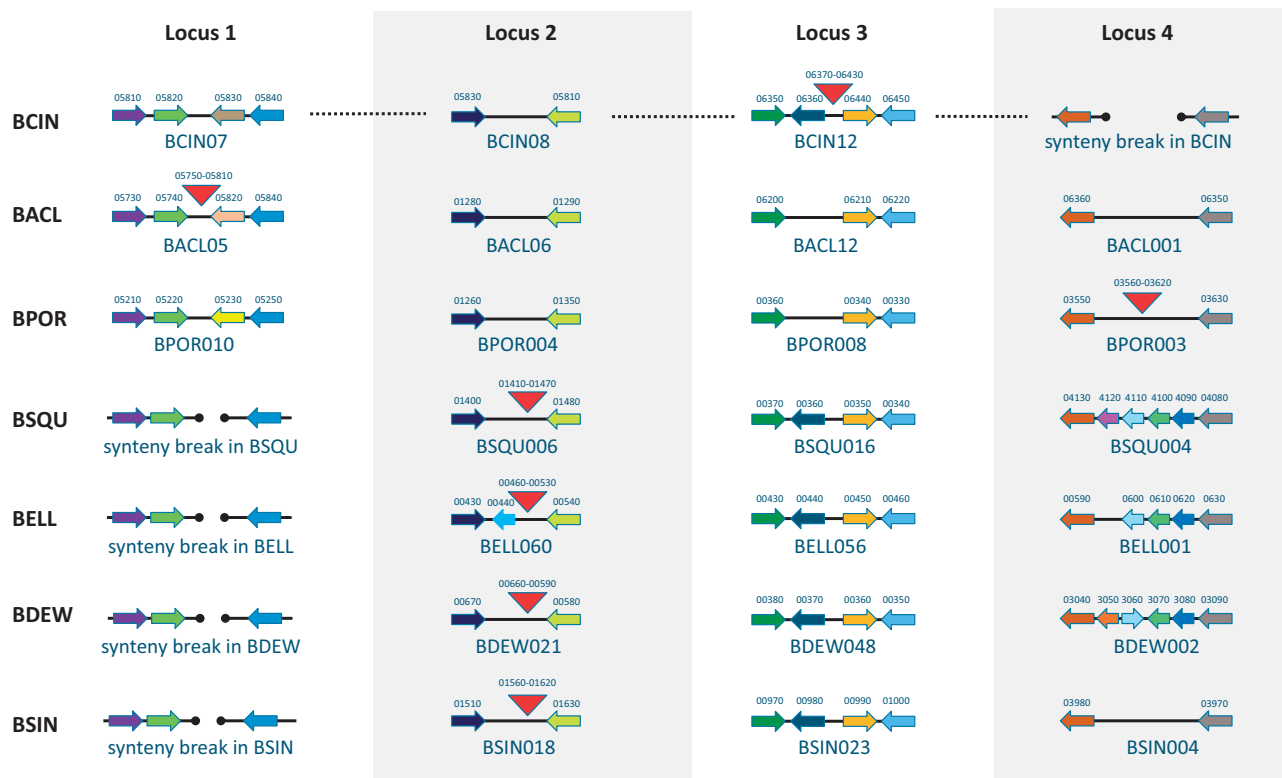
Fig. 6.—Distinct genomic locations of BOT clusters in seven *Botrytis* species. Four different loci are provided in the columns. Species name tags are in the left hand margin: BCIN, *B. cinerea*; BACL, *B. aclada*; BPOR, *B. porri*; BSIN, *B. sinoallii*; BSQU, *B. squamosa*; BDEW, *B. deweyae*; BELL, *B. elliptica*. Contig numbers in the seven species are provided underneath the locus. In each column, orthologous genes are indicated by identical colors. Gene numbers in the contig are provided above the gene; the arrow indicates direction of transcription. The red triangular blocks represent the location of a BOT cluster. Synteny breaks are shown by interrupted lines with dots marking the break.

In *Sclerotinia sclerotiorum*, the BOA cluster is dispersed over two chromosomal locations on SSCL05 (genes BOA1 and BOA2) and SSCL15 (genes BOA3-13). A recent study by Graham-Taylor et al. (2020) reported that SSCL can express the 13 BOA genes in a coregulated manner despite their spatial separation. For the largest cluster on SSCL15, its flanking genes on both sides are orthologous to syntenic regions in eight *Botrytis* species (BACL006, BBYS014, BCIN06, BDEW005, BELL059, BGLO010, BSIN006, and BSQU018) that do not contain any trace of BOA gene remnants. For the smaller cluster on SSCL05, its flanking genes on both sides are orthologous to genes located on BCIN05 (Bcin05g05060 and Bcin05g07100); however, the region is not syntenic, because the genes are far separated in *B. cinerea*.

Inheritance and Structural Evolution of BOT and BOA Clusters

BOT and BOA gene loci were carefully examined for evidence of pseudogenization to infer which of the clusters are fully functional (supplementary data S5 and S6, Supplementary Material online). BOT clusters in *B. sinoallii* and *B. paeoniae* contain one and two pseudogenes, respectively, whereas six

species (*B. aclada*, *B. cinerea*, *B. elliptica*, *B. deweyae*, *B. porri*, and *B. squamosa*) have clusters with seven apparently functional genes (supplementary data S5, Supplementary Material online). Seventeen of the 19 Sclerotiniaceae analyzed contained (parts of) BOA clusters, however only seven species (*B. aclada*, *B. byssoidea*, *B. cinerea*, *B. globosa*, *B. porri*, *B. sinoallii*, and *Sclerotinia sclerotiorum*) appeared to contain a fully functional BGC (supplementary data S6, Supplementary Material online). The majority of species contain two or more pseudogenes of catalytic enzymes. The most extreme cases of gene loss were in *B. squamosa*, *B. deweyae*, *B. elliptica*, and *B. tulipae*, which lost all but one of the BOA cluster genes. By contrast, *B. calthae*, *B. convoluta*, and *B. narcissicola* contained 2–3 pseudogenes, either in genes encoding accessory enzymes or in the BOA13 gene, which is the transcriptional regulator for the cluster (Porquier et al. 2019). Of the two species outside the genus *Botrytis*, *Sclerotinia sclerotiorum* contains a functional BOA cluster (Graham-Taylor et al. 2020), whereas *S. cepivorum* lacks four genes, including polyketide synthase gene BOA9, and in addition contains two pseudogenes.

Ancestral state reconstructions of genes and pseudogenes (considering HGT events, see below) on the *Botrytis* species

A botrydial cluster

B botcinic acid cluster

cluster status

- functional vertical
- functional horizontal
- non-functional all pseudogenes/absent
- non-functional multiple gene states

ancestral gene state

- functional vertical
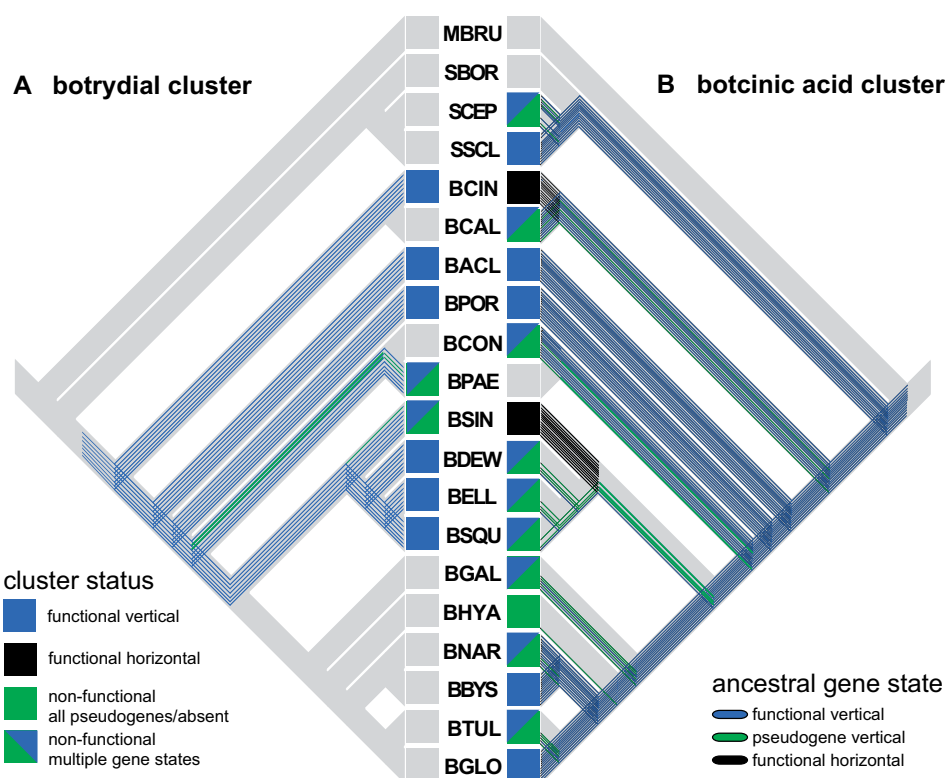- pseudogene vertical
- functional horizontal

FIG. 7.—Ancestral state reconstructions of genes and pseudogenes of the BOT cluster (A) and the BOA cluster (B) on the phylogenetic tree of 20 Sclerotiniaceae species. The status of the cluster is indicated with colored boxes: blue = functional cluster, vertically transmitted; black = functional cluster, horizontally transmitted; green = all cluster genes nonfunctional or absent; green/blue = some genes nonfunctional or absent; gray = total absence of cluster. The ancestral gene states of seven BOT genes and 13 BOA genes are indicated with colored lines in similar way.

tree (fig. 7) suggest that the BOT cluster was gained in the common ancestor of *Botrytis* and has been lost five times; three times leaving no gene remnants (in *B. calthae*, *B. convolute*, and in the subclade containing *B. galanthina*), and twice leaving a mix of functional genes and pseudogenes (in *B. paeoniae* and *B. sinoallii*). The BOT gene trees (supplementary data S7, Supplementary Material online) are in agreement with the species tree and the clusters are thus inferred to be derived from strictly vertical inheritance. Reconstructions of the BOA clusters (fig. 7) revealed a more dynamic process involving 12 losses of cluster function after being gained in the common ancestor of *Botrytis* and *Sclerotinia*, and two recent gains by HGT in *B. cinerea* and *B. sinoallii*. HGT of the two clusters is supported by maximum-likelihood gene trees (supplementary data S8, Supplementary Material online), which suggests that both clusters were acquired from a relative of *B. porri* or *B. aclada*.

Most gene trees became significantly worse than the maximum-likelihood trees, according to Approximately Unbiased tests (Shimodaira 2002), when potential HGT homologs were excluded from the putative donor clade (supplementary data S9, Supplementary Material online). Strong support for a HGT origin of the functional BOA cluster in

B. sinoallii comes from two additional observations. First, the inferred HGT cluster is adjoined by a putative amino acid transporter (Bsin003g06700) and alcohol acetyltransfer-ase (Bsin003g06560), which are either adjacent or a few genes removed from the BOA cluster in *B. aclada*; only the homolog of Bsin003g06700 is adjacent to the BOA cluster in *B. porri* (supplementary data S10, Supplementary Material online). Second, *B. sinoallii* contains an additional, heavily pseudogenized BOA cluster on contig BSIN027, which more closely tracks the species phylogeny (supplementary data S8, Supplementary Material online) and retains flanking genes that are consistent with the species phylogeny (supplementary data S10, Supplementary Material online). The remnants of the ancestral *B. sinoallii* BOA cluster comprise only three pseudogenes that are embedded in a 330-kb genomic region saturated with transposons.

The HGT of the BOA cluster to *B. cinerea* is supported by the phylogenetic proximity to *B. aclada* and *B. porri* (fig.7; supplementary data S8, Supplementary Material online), however, it cannot be corroborated by synteny information, as the *B. cinerea* BOA cluster is located at the start of chromosome 1, and the 25-kb region immediately downstream of the cluster is not syntenic with any *Botrytis* species.

Discussion

Following the efforts to sequence *B. cinerea* isolate B05.10 and nine other *Botrytis* species mainly infecting flower bulb crops (Valero-Jiménez et al. 2019), the present study, focusing on eight species from clade 2 of the genus, brings the number of *Botrytis* genome sequences to 16. This represents about half of the currently recognized species in the genus, though a recent study (Garfinkel et al. 2019) identified at least 15 phylogenetically distinct, new taxa sampled from *Paeonia* in Alaska, which remain to be described and named. There is thus far one single fungal genus, that is, *Verticillium*, for which the genomes of all recognized species have been sequenced (Shi-Kunne et al. 2018). It will take more effort to complete the sequencing of the entire genus *Botrytis.*

The present study aimed to identify genes potentially involved in determining host specificity, by comparing genomes of *Botrytis* species pathogenic on *Allium* with each other and with the genomes of their closest relatives pathogenic on other host plants. Specifically, we compared the genomes of the onion (*Allium cepa*) pathogens *B. squamosa* and *B. sinoallii*, with those of their sister taxa *B. elliptica* and *B. deweyae*, which infect lily and *Hemerocallis*, respectively, and we compared the genomes of *B. aclada* (infecting onion) and *B. porri* (infecting *Allium porri*, leek) with that of *B. paeoniae* (infecting the dicot peony). In order to make a meaningful comparison, the effort was made of manually curating all (>11,000) gene models in the genomes of three species (*B. squamosa*, *B. aclada*, and *S. cepivorum*), and manually curating the gene models of all proteins with a (predicted) signal peptide in the other six species. Comparison of the effector repertoires did not reveal candidate effectors that were shared among all *Allium* pathogens but absent in non-*Allium* pathogens. Each of the species analyzed contained 8–39 predicted effector genes that were unique to the species, however, most had no homologs in other fungi and these genes often had little RNA-Seq support (even in RNA samples from infected onion tissue), questioning the importance of these predicted genes for pathogenicity on onion. The repertoire of cell wall degrading enzymes was also similar between all 16 *Botrytis* species studied, despite the fact that only three species infect dicot hosts, whereas the vast majority infect monocot hosts. Dicots and monocots are considered to have different compositions of cell wall polysaccharides (Jarvis et al. 1988). Thirteen *Botrytis* species in this study infect monocot hosts from the families *Alliaceae*, *Amaryllidaceae*, *Iridaceae*, and *Liliaceae*. Plants from these families contain high levels of pectin in their cell walls as compared with the *Poaceae* (Jarvis et al. 1988), which are more intensively studied as they comprise major staple crops of global relevance: rice, wheat, and maize. In view of the high pectin content in the monocot hosts of *Botrytis* species in this study, the large repertoire of pectin degrading enzymes in their genomes appears logical. Altogether, we did not identify (sets of) genes

that are shared among the *Allium* pathogens and distinguish them from related species with different hosts. The lack of shared genomic features may reflect the pathology of the *Allium* pathogens, some of which infect the leaves (*B. squamosa*), whereas others infect the bulb (*B. aclada*) or the roots and scale bases (*S. cepivorum*).

Despite the failure to identify host specificity determinants, many interesting features were unraveled by the extensive genome analyses that were performed. The genome of *B. aclada* was assembled into 16 gapless chromosomes, eight of which were full-length (telomere-to-telomere) and six contained telomeric repeats on one end. The *B. aclada* assembly was based on sufficiently high coverage to avoid the requirement for short-read-based correction, nor did it require an optical map or genetic map for assembly verification, as was done for *B. cinerea* (van Kan et al. 2017). Cytogenetic studies on four *Botrytis* species (*B. byssoidea*, *B. cinerea*, *B. squamosa*, and *B. tulipae*) revealed that they each contain 16 mitotic chromosomes, whereas the same study reported 16 or 32 mitotic chromosomes in different isolates of *B. allii* (Shirane et al. 1989). Subsequent studies (Nielsen and Yohalem 2001; Yohalem et al. 2003) revealed that the species earlier named *B. allii* in fact comprised isolates of *B. aclada* (having 16 chromosomes) as well as isolates representing a hybrid of *B. byssoidea* and *B. aclada* (having 32 chromosomes), which is presently still named as *B. allii* (Staats et al. 2005). Strikingly, *Sclerotinia sclerotiorum* also contains 16 chromosomes (Amselem et al. 2011; Derbyshire et al. 2017). These observations suggest a bias for the possession of 16 chromosomes in the genus *Botrytis* and possibly even in related genera. Conservation of chromosome numbers is not commonly observed in fungal genera, especially Ascomycota. As an example, the core chromosome numbers in the genus *Fusarium* vary from four (*Fusarium graminearum*) to 12 (*Fusarium fujikuroi*) (Waalwijk et al. 2018). Could this conservation of chromosome numbers in distant species of the same genus be related to functional constraints for sexual reproduction during the evolution of *Botrytis* species? As sexual reproduction requires chromosome pairing during meiosis, any fusion or fission event that affects core chromosome numbers would have serious repercussion on sexual compatibility and the fertility of offspring. We further explored the conservation of chromosome numbers and architecture by examining synteny and reconstructing ancestral genomes of the genus *Botrytis* and the family Sclerotiniaceae.

The ancestral genome reconstruction inferred as few as 17 syntenic blocks for the common ancestor (AB0) of all *Botrytis* species. The inferred ancestral genome of the Sclerotiniaceae (ABS0) consisted of 16 syntenic blocks, and it differed from the AB0 genome by a single rearrangement. Thirteen of the 16 core chromosomes of *B. cinerea* were represented in these blocks, and only three interchromosomal rearrangements were proposed between the ancestor AB0 and the extant *B. cinerea* genome. Moreover, the common ancestor of the

entire genus (AB0) was identical to the common ancestor of extant *Botrytis* species in clade 2. Only six interchromosomal rearrangements were proposed between the genome of ancestor A1 and the extant *B. aclada* genome. The genomes of *B. cinerea* and *B. aclada* were thus remarkably syntenic, considering the phylogenetic distance between the two species. Representatives of the two clades within the genus *Botrytis* (Staats et al. 2005) were recently included in molecular clock-based estimates of divergence times for Ascomycota, and these species were estimated to have diverged 5.9 Ma (Shen et al. 2020). The maintenance of 16 chromosomes and the stability of their overall configuration would facilitate chromosome pairing during meiosis. This observation thus suggests the occurrence of a strong selection pressure on sexual reproduction within the genus *Botrytis* over time. The suggestion is further supported by the fact that *Sclerotinia sclerotiorum* also possesses 16 chromosomes (Derbyshire et al. 2017) and that the ancestral genome of the Sclerotiniaceae differs from the ancestral *Botrytis* genome only by a single rearrangement, despite the divergence between the genera *Sclerotinia* and *Botrytis* being estimated to have occurred around 21.5 Ma (Shen et al. 2020). The extent of synteny among *Botrytis* species from distinct clades could only have been retained if sexual reproduction in this genus has been prominent over the course of evolution. Of the 22 *Botrytis* species used in the initial phylogeny of the genus (Staats et al. 2005), 14 were reported to have a sexual stage, whereas eight were not, including *B. aclada.* Population studies may shed more light on the modes of reproduction of *Botrytis* species. Thus far, only *B. cinerea*, *B. pseudocinerea*, *B. tulipae*, and *B. elliptica* have been subject of population analyses (Giraud et al. 1999; Fournier et al. 2005; Staats et al. 2007; Walker et al. 2015; Mercier et al. 2019; Soltis et al. 2019), whereas other species have received less attention.

Although synteny analyses indicated a strong overall conservation of chromosome architecture between *Botrytis* species, it was striking to detect a substantial number of small translocations between *B. cinerea* and *B. aclada*, both in telomeric and internal chromosomal regions. Telomeric translocations are relatively "safe" rearrangements, as they have limited impact on genome architecture and chromatin organization, minimizing the risk of causing major genome stress. However, such rearrangements have the potential risk of (partial or complete) loss of the telomeric region during the translocation. The BOA clusters that were detected in multiple *Botrytis* species were, with two exceptions, located at the end of contigs, presumably because they were flanked by repetitive sequences. In *Sclerotinia sclerotiorum*, however, the BOA cluster is located internally in chromosome SSCLE15, and it is not flanked by repetitive sequences. Although it seems logical to propose a role of repetitive sequences in the translocation of chromosomal segments (whether telomeric or internal), further studies need to

establish such a role. Sequencing multiple isolates of some of the species by long-read technology might reveal the frequency of translocation events within a species.

It was remarkable to note that the BOT clusters appears to be located in four distinct genomic locations in the seven *Botrytis* species in which it was analyzed, and each of the loci was flanked by transposons, and in three cases even interrupted by transposons. It is tempting to speculate that these transposons have played a role in the mobility of the BOT cluster within the genome. The phylogeny of the BOT gene clusters was in full agreement with the species phylogeny, arguing against a horizontal transfer event. Thus, the data suggest that there have been independent translocations of the BOT gene cluster to distinct chromosomes, culminating in the four distinct genomic locations presently observed in extant fungal isolates. Only within *B. squamosa*, *B. deweyae*, and *B. elliptica* was the BOT cluster in the equivalent genomic location, as could be expected from their phylogenetic proximity within a subclade of clade 2. This suggests a unique transposition event in the lineage toward the common ancestor of species in this subclade (A5 in fig. 4). It is not currently possible to estimate the timing of these translocations, nor could the position of the BOT cluster in the ancestral genome be inferred in the Anchro analysis.

Polymorphism in genomic locations of SM BGCs was recently described within a collection of *Aspergillus fumigatus* isolates, suggesting that mobility of BGCs may occur even within a single species. In this study, there was even one case of two isolates carrying idiomorph BGCs, that is, two distinct clusters residing in the same genomic locations (Lind et al. 2017). It will be interesting to analyze multiple isolates of the different *Botrytis* species and explore whether mobility of BGCs occurs within a single species as well. Long-read sequence technology will be essential for such purpose, to obtain flanking sequence information that permits to infer the correct genomic locations of the various BGCs.

The Evolution and Dynamics of BOT and BOA Clusters

The BGCs involved in the production of phytotoxic SMs BOT and BOA were specifically interesting because they trigger (programmed) cell death in dicots (Rossi et al. 2011) and in monocots (our unpublished results) and contribute to the virulence of *B. cinerea* (Dalmais et al. 2011). The unusual observation of the distinct genomic locations of BOT and BOA clusters encouraged us to explore two distinct evolutionary scenarios: that either clusters were vertically transmitted but were able to excise from their location and reinsert at distinct locations; or that clusters were lost and then regained through HGT. We carefully evaluated the functionality, synteny, and phylogeny of BOT and BOA genes and avoided assuming that vertical gene duplication is the source of multiple paralogs within a lineage. Indeed, half the BOA clusters inferred to be functional in *Botrytis* appear to have been acquired by

HGT from other *Botrytis* species, and the functional BOA cluster in *B. sinoallii* is inferred to be a xenolog (horizontally acquired paralog) of the pseudogenized cluster in the same species. The fact that the inferred donor of the BOA cluster in *B. sinoallii* (a taxon closely related to *B. aclada* and *B. porri*), which also is a pathogen of *Allium*, is consistent with host-specific functions selecting for cluster HGT. BGC birth and death processes appear to involve the horizontal replacement of commonly lost clusters; however, the trajectories of BOT and BOA contrast in their evolutionary dynamics. Although BOT is less frequently lost/nonfunctionalized and has not been gained by HGT in this data set, BOA is frequently lost or non-functionalized and also replaced by HGT. It is possible that BOT is more readily retained by natural selection due to its role in microbial competition (Vignatti et al. 2020).

This genome comparison has not revealed any host range determinants that enable so many *Botrytis* species (and *S. cepivorum*) to infect *Allium* hosts, likely because fungus–plant interactions may depend on a multitude of factors. Especially the fact that some of these species infect leaf tissue, whereas others infect the bulb or the root, and some species induce blight symptoms, whereas others cause maceration and rot, adds another layer of complexity when comparing species pathogenic on the same host. The high synteny and conservation of chromosome architecture between such distant species across the genus *Botrytis* is remarkable and contrasts with the dynamics of genome evolution in many other plant pathogens.

Supplementary Material

Supplementary data are available at *Genome Biology and Evolution* online.

Acknowledgments

Data Availability

The project has been deposited in GenBank under the Bioproject number PRJNA494516. The Biosamples related to this project have accession numbers SAMN10219759–SAMN10219767. The raw PacBio genomic read data are deposited under accession numbers SRR8062108–SRR8062116. Assembled genomes are deposited with accession numbers

RCSV00000000	SAMN10219759	BOTACL
RCSW00000000	SAMN10219760	BOTBYS
RCSX00000000	SAMN10219761	BOTDEW
RCSY00000000	SAMN10219762	BOTELL
RCSZ00000000	SAMN10219763	BOTGLO
RCTA00000000	SAMN10219764	BOTPOR
RCTB00000000	SAMN10219765	BOTSIN
RCTC00000000	SAMN10219766	BOTSQU
RCTD00000000	SAMN10219767	SCLCEP

The 12 RNA-Seq data used for gene prediction are deposited in GenBank under Bioproject number PRJNA494516, with sequence accession numbers SRR8053381–SRR8053392.

Literature Cited

Amselem J, et al. 2011. Genomic analysis of the necrotrophic fungal pathogens *Sclerotinia sclerotiorum* and *Botrytis cinerea*. PLoS Genet. 7(8):e1002230.

Ashton PM, et al. 2019. Three phylogenetic groups have driven the recent population expansion of *Cryptococcus neoformans*. Nat Commun. 10:2035.

Bertazzoni S, et al. 2018. Accessories make the outfit: accessory chromosomes and other dispensable DNA regions in plant-pathogenic fungi. Mol Plant Microbe Interact. 31(8):779–788.

Campbell MA, Rokas A, Slot JC. 2012. Horizontal transfer and death of a fungal secondary metabolic gene cluster. Genome Biol Evol. 4(3):289–293.

Cantarel BL, et al. 2008. MAKER: an easy-to-use annotation pipeline designed for emerging model organism genomes. Genome Res. 18(1):188–196.

Capella-Gutiérrez S, Silla-Martínez JM, Gabaldón T. 2009. trimAl: a tool for automated alignment trimming in large-scale phylogenetic analyses. Bioinformatics 25:1972–1973.

Chakraborty M, Baldwin-Brown JG, Long AD, Emerson JJ. 2016. Contiguous and accurate de novo assembly of metazoan genomes with modest long read coverage. Nucleic Acids Res. 44:e147.

Chatterjee S, Kuang Y, Splivallo R, Chatterjee P, Karlovsky P. 2016. Interactions among filamentous fungi *Aspergillus niger*, *Fusarium verticillioides* and *Clonostachys rosea*: fungal biomass, diversity of secreted metabolites and fumonisin production. BMC Microbiol. 16:83.

Chin CS, et al. 2013. Nonhybrid finished microbial genome assemblies from long-read SMRT sequencing data. Nat Methods. 10(6):563–569.

Contreras-Moreira B, Vinuesa P. 2013. GET_HOMOLOGUES, a versatile software package for scalable and robust microbial pangenome analysis. Appl Environ Microbiol. 79:7696–7701.

Dalmais B, et al. 2011. The *Botrytis cinerea* phytotoxin botcinic acid requires two polyketide synthases for production and has a redundant role in virulence with botrydial. Mol Plant Pathol. 12(6):564–579.

de Vries RP, et al. 2017. Comparative genomics reveals high biological diversity and specific adaptations in the industrially and medically important fungal genus *Aspergillus*. Genome Biol. 18:28.

Derbyshire M, et al. 2017. The finished genome of the plant-infecting fungus *Sclerotinia sclerotiorum*: re-visiting the 'two-speed-genome' hypothesis in the context of broad host-range plant pathogenesis. Genome Biol Evol. 9(3):593–618.

Dong S, Raffaele S, Kamoun S. 2015. The two-speed genomes of filamentous pathogens: waltz with plants. Curr Opin Genet Dev. 35:57–65.

Dunn NA, et al. 2019. Apollo: democratizing genome annotation. PLoS Comput Biol. 15(2):e1006790.

Edgar RC. 2010. Search and clustering orders of magnitude faster than BLAST. Bioinformatics 26(19):2460–2461.

Elad Y, Pertot I, Cotes Prado AM, Stewart A. 2016. Plant hosts of *Botrytis* spp. In: Fillinger S, Elad Y, editors. Botrytis: the fungus, the pathogen and its management in agricultural systems. Cham (Switzerland): Springer International Publishing. p. 413–86.

Emanuelsson O, Brunak S, von Heijne G, Nielsen H. 2007. Locating proteins in the cell using TargetP, SignalP and related tools. Nat Protoc. 2:953–971.

Emms DM, Kelly S. 2015. OrthoFinder: solving fundamental biases in whole genome comparisons dramatically improves orthogroup inference accuracy. Genome Biol. 16(1):157.

Faris JD, et al. 2010. A unique wheat disease resistance-like gene governs effector-triggered susceptibility to necrotrophic pathogens. Proc Natl Acad Sci U S A. 107(30):13544–13549.

Fournier E, Giraud T, Albertini C, Brygoo Y. 2005. Partition of the *Botrytis cinerea* complex in France using multiple gene genealogies. Mycologia 97(6):1251–1267.

Friesen TL, et al. 2006. Emergence of a new disease as a result of interspecific virulence gene transfer. Nat Genet. 38(8):953–956.

Garfinkel AR, Coats KP, Sherry DL, Chastagner GA. 2019. Genetic analysis reveals unprecedented diversity of a globally-important plant pathogenic genus. Sci Rep. 9(1):6671.

Garfinkel AR, Lorenzini M, Zapparoli G, Chastagner GA. 2017. *Botrytis euroamericana*, a new species from peony and grape in North America and Europe. Mycologia 109:495–507.

Giraud T, et al. 1999. Two sibling species of the *Botrytis cinerea* complex, transposa and vacuma, are found in sympatry on numerous host plants. Phytopathology 89(10):967–973.

Gluck-Thaler E, Slot JC. 2018. Specialized plant biochemistry drives gene clustering in fungi. ISME J. 12(7):1694–1705.

Graham-Taylor C, Kamphuis LG, Derbyshire MC. 2020. A detailed *in silico* analysis of secondary metabolite biosynthesis clusters in the genome of the broad host range plant pathogenic fungus *Sclerotinia sclerotiorum*. BMC Genomics. 21(1):7.

Grant-Downton RT, et al. 2014. A novel *Botrytis* species is associated with a newly emergent foliar disease in cultivated *Hemerocallis*. PLoS One 9(6):e0089272.

Hoff KJ, Lange S, Lomsadze A, Borodovsky M, Stanke M. 2016. BRAKER1: unsupervised RNA-Seq-based genome annotation with Genemark-ET and Augustus. Bioinformatics 32(5):767–769.

Hyde KD, et al. 2014. One stop shop: backbones trees for important phytopathogenic genera. Fungal Divers. 67(1):21–125.

Jarvis MC, Forsyth W, Duncan HJ. 1988. A survey of the pectic content of nonlignified monocot cell walls. Plant Physiol. 88(2):309–314.

Katoh K, Standley DM. 2013. MAFFT multiple sequence alignment software version 7: improvements in performance and usability. Mol Biol Evol. 30(4):772–780.

Keller NP, Turner G, Bennett JW. 2005. Fungal secondary metabolism—from biochemistry to genomics. Nat Rev Microbiol. 3(12):937–947.

Koren S, Walenz BP, Berlin K, Miller JR, Phillippy AM. 2017. Canu: scalable and accurate long-read assembly via adaptive k-mer weighting and repeat separation. Genome Res. 27:1–15.

Krogh A, Larsson B, von Heijne G, Sonnhammer EL. 2001. Predicting transmembrane protein topology with a hidden Markov model: application to complete genomes. J Mol Biol. 305(3):567–580.

Li L. 2003. OrthoMCL: identification of ortholog groups for eukaryotic genomes. Genome Res. 13(9):2178–2189.

Lind A, et al. 2017. Drivers of genetic diversity in secondary metabolic gene clusters within a fungal species. PLoS Biol. 15(11):e2003583.

Liu ZH, et al. 2009. SnTox3 acts in effector triggered susceptibility to induce disease on wheat carrying the Snn3 gene. PLoS Pathog. 5(9):e1000581.

Liu ZH, et al. 2012. The cysteine rich necrotrophic effector SnTox1 produced by *Stagonospora nodorum* triggers susceptibility of wheat lines harboring Snn1. PLoS Pathog. 8(1):e1002467.

Lo Presti L, Kahmann R. 2017. How filamentous plant pathogen effectors are translocated to host cells. Curr Opin Plant Biol. 38:19–24.

Love J, et al. 2019. nextgenusfs/funannotate: funannotate v1.5.3 Version 1.5.3. Available from: https://github.com/nextgenusfs/funannotate. Accessed June 2018.

Maddison WP, Maddison DR. 2019. Mesquite: a modular system for evolutionary analysis. Version 3.61. Available from: http://www.mesquiteproject.org. Accessed July 2020.

McDonald MC, et al. 2019. Transposon-mediated horizontal transfer of the host-specific virulence protein ToxA between three fungal wheat pathogens. mBIO 10(5):e01515.

Medema MH, et al. 2015. Minimum information about a biosynthetic gene cluster. Nat Chem Biol. 11:625–631.

Mercier A, et al. 2019. The polyphagous plant pathogenic fungus *Botrytis cinerea* encompasses host-specialized and generalist populations. Environ Microbiol. 21(12):4808–4821.

Min B, Grigoriev IV, Choi IG. 2017. FunGAP: Fungal Genome Annotation Pipeline using evidence-based gene model evaluation. Bioinformatics 33(18):2936–2937.

Möller M, Stukenbrock EH. 2017. Evolution and genome architecture in fungal plant pathogens. Nat Rev Microbiol. 15(12):756–771.

Navarro-Munoz JC, Collemare JM. 2020. Evolutionary histories of type III polyketide synthases in fungi. Front Microbiol. 10:3018.

Navarro-Muñoz JC, et al. 2020. A computational framework to explore large-scale biosynthetic diversity. Nat Chem Biol. 16(1):60–68.

Nguyen LT, Schmidt HA, von Haeseler A, Minh BQ. 2015. IQ-TREE: a fast and effective stochastic algorithm for estimating maximum-likelihood phylogenies. Mol Biol Evol. 32(1):268–274.

Nielsen K, Yohalem DS. 2001. Origin of a polyploid *Botrytis* pathogen through interspecific hybridization between *Botrytis aclada* and *B. byssoidea*. Mycologia 93(6):1064–1071.

Pedro H, Yates AD, Kersey PJ, De Silva NH. 2019. Collaborative annotation redefines gene sets for crucial phytopathogens. Front Microbiol. 10:2477.

Petersen TN, Brunak S, von Heijne G, Nielsen H. 2011. SignalP 4.0: discriminating signal peptides from transmembrane regions. Nat Methods. 8(10):785–786.

Pinedo C, et al. 2008. Sesquiterpene synthase from the botrydial biosynthetic gene cluster of the phytopathogen *Botrytis cinerea*. ACS Chem Biol. 3(12):791–801.

Porquier A, et al. 2016. The botrydial biosynthetic gene cluster of *Botrytis cinerea* displays a bipartite genomic structure and is positively regulated by the putative Zn(II)(2)Cys(6) transcription factor BcBot6. Fung Genet Biol. 96:33–46.

Porquier A, et al. 2019. Botcinic acid biosynthesis in *Botrytis cinerea* relies on a subtelomeric gene cluster surrounded by relics of transposons and is regulated by the Zn(2)Cys(6) transcription factor BcBoa13. Curr Genet. 65(4):965–980.

Reynolds HT, et al. 2018. Horizontal gene cluster transfer increased hallucinogenic mushroom diversity. Evol Lett. 2(2):88–101.

Ropars J, et al. 2015. Adaptive horizontal gene transfers between multiple cheese-associated fungi. Curr Biol. 25(19):2562–2569.

Rossi FR, et al. 2011. The sesquiterpene botrydial produced by *Botrytis cinerea* induces the hypersensitive response on plant tissues and its action is modulated by salicylic acid and jasmonic acid signaling. Mol Plant Microbe Interact. 24(8):888–896.

Shannon P, et al. 2003. Cytoscape: a software environment for integrated models of biomolecular interaction networks. Genome Res. 13(11):2498–2504.

Shen XX, et al. 2020. Genome-scale phylogeny and contrasting modes of genome evolution in the fungal phylum Ascomycota. BioRxiv. Available from: https://doi.org/10.1101/2020.05.11.088658.

Shi GJ, et al. 2015. The wheat Snn7 gene confers susceptibility on recognition of the *Parastagonospora nodorum* necrotrophic effector SnTox7. Plant Genome 8(2):1–10.

Shi GJ, et al. 2016. Marker development, saturation mapping, and high-resolution mapping of the Septoria nodorum blotch susceptibility gene Snn3-B1 in wheat. Mol Genet Genomics. 291(1):107–119.

Shi-Kunne X, Faino L, van den Berg GCM, Thomma BPHJ, Seidl MF. 2018. Evolution within the fungal genus *Verticillium* is characterized by chromosomal rearrangement and gene loss. Environ Microbiol. 20(4):1362–1373.

Shimodaira H. 2002. An approximately unbiased test of phylogenetic tree selection. Syst Biol. 51(3):492–508.

Shirane N, Masuko M, Hayashi Y. 1989. Light microscopic observation of nuclei and mitotic chromosomes of *Botrytis* species. Phytopathology 79(7):728–730.

Siewers V, et al. 2005. Functional analysis of the cytochrome P450 monooxygenase gene bcbot1 of *Botrytis cinerea* indicates that botrydial is a strain-specific virulence factor. Mol Plant Microbe Interact. 18(6):602–612.

Simão FA, Waterhouse RM, Ioannidis P, Kriventseva EV, Zdobnov EM. 2015. BUSCO: assessing genome assembly and annotation completeness with single-copy orthologs. Bioinformatics 31(19):3210–3212.

Sipos G, et al. 2017. Genome expansion and lineage-specific genetic innovations in the forest pathogenic fungi Armillaria. Nat Ecol Evol. 1(12):1931–1941.

Slot J, Gluck-Thaler E. 2019. Metabolic gene clusters, fungal diversity, and the generation of accessory functions. Curr Opinion Genet Dev. 58:17–24.

Soltis NE, et al. 2019. Interactions of tomato and *Botrytis cinerea* genetic diversity: parsing the contributions of host differentiation, domestication, and pathogen variation. Plant Cell 31(2):502–519.

Spatafora JW, et al. 2017. The fungal tree of life: from molecular systematics to genome-scale phylogenies. Microbiol Spectr. 5.

Sperschneider J, et al. 2016. EffectorP: predicting fungal effector proteins from secretomes using machine learning. New Phytol. 210(2):743–761.

Staats M, van Baarlen P, van Kan JAL. 2005. Molecular phylogeny of the plant pathogenic genus *Botrytis* and the evolution of host specificity. Mol Biol Evol. 22(2):333–346.

Staats M, van Baarlen P, van Kan JAL. 2007. AFLP analysis of genetic diversity in populations of *Botrytis elliptica* and *Botrytis tulipae* from the Netherlands. Eur J Plant Pathol. 117(3):219–235.

Stamatakis A. 2014. RAxML version 8: a tool for phylogenetic analysis and post-analysis of large phylogenies. Bioinformatics 30(9):1312–1313.

Stanke M, Schöffmann O, Morgenstern B, Waack S. 2006. Gene prediction in eukaryotes with a generalized hidden Markov model that uses hints from external sources. BMC Bioinf. 7(1):62.

Vakirlis N, et al. 2016. Reconstruction of ancestral chromosome architecture and gene repertoire reveals principles of genome evolution in a model yeast genus. Genome Res. 26(7):918–932.

Valero-Jiménez C, Veloso J, Staats M, van Kan JAL. 2019. Comparative genomics of plant pathogenic *Botrytis* species with distinct host specificity. BMC Genomics. 20(1):203.

van Kan JAL, et al. 2017. A gapless genome sequence of the fungus *Botrytis cinerea*. Mol Plant Pathol. 18(1):75–89.

Veloso J, van Kan JAL. 2018. Many shades of grey in *Botrytis*-host plant interactions. Trends Plant Sci. 23(7):613–622.

Vignatti P, et al. 2020. Botrydial confers *Botrytis cinerea* the ability to antagonize soil and phyllospheric bacteria. Fung Biol. 124(1):54–64.

Waalwijk C, et al. 2018. Karyotype evolution in *Fusarium*. IMA Fungus 9(1):13–26.

Walker AS, et al. 2015. Population structure and temporal maintenance of the multihost fungal pathogen *Botrytis cinerea*: causes and implications for disease management. Environ Microbiol. 17(4):1261–1274.

Weber T, et al. 2015. antiSMASH 3.0—a comprehensive resource for the genome mining of biosynthetic gene clusters. Nucleic Acids Res. 43(W1):W237–W243.

Yohalem DS, Nielsen K, Nicolaisen M. 2003. Taxonomic and nomenclatural clarification of the onion neck rotting *Botrytis* species. Mycotaxon 85:175–182.

Associate editor: Li-Jun Ma